

# Resonant ion-dip infrared spectroscopy of benzene–H<sub>2</sub>O and benzene–HOD

R. Nathaniel Pribble, Aaron W. Garrett, Kenneth Haber, and Timothy S. Zwier<sup>a)</sup>  
*Department of Chemistry, Purdue University, West Lafayette, Indiana 47907-1393 and The Joint Institute  
for Laboratory Astrophysics, The University of Colorado, Boulder, Colorado 80309*

(Received 16 February 1995; accepted 4 April 1995)

Resonant ion-dip infrared spectra of C<sub>6</sub>H<sub>6</sub>–H<sub>2</sub>O and C<sub>6</sub>H<sub>6</sub>–HOD have been recorded in the OH stretch fundamental region. The spectra provide further evidence for the unique, large-amplitude motions present in these  $\pi$  hydrogen-bonded complexes. In C<sub>6</sub>H<sub>6</sub>–H<sub>2</sub>O, transitions out of the lowest ortho ( $\Pi$ ) and para ( $\Sigma$ ) ground state levels are observed. A transition at 3634 cm<sup>-1</sup> is assigned as an unresolved pair of parallel transitions ( $\Sigma \rightarrow \Sigma$  and  $\Pi \rightarrow \Pi$ ) involving the symmetric stretch fundamental (at 3657 cm<sup>-1</sup> in free H<sub>2</sub>O). In the antisymmetric stretch region, transitions at 3713, 3748, and 3774 cm<sup>-1</sup> are assigned as  $\Pi \rightarrow \Sigma$ ,  $\Sigma \rightarrow \Pi$ , and  $\Pi \rightarrow \Delta$  transitions, respectively. The spacing of the transitions is consistent with nearly free internal rotation of H<sub>2</sub>O about benzene's sixfold axis in both ground and vibrationally excited states. The intensities of combination bands depends critically on the mixing of some local mode character into the symmetric and antisymmetric stretches at asymmetric positions of H<sub>2</sub>O on benzene. Surprisingly, in C<sub>6</sub>H<sub>6</sub>–HOD, five transitions are observed in the OH stretch region, all arising from the ground state zero point level. Even more unusual, the higher-energy combination bands are many times stronger than the OH stretch fundamental. The local mode OH stretch has components both parallel and perpendicular to benzene's sixfold axis, leading to strong parallel and perpendicular transitions in the spectrum. A two-dimensional model involving free internal rotation and torsion of HOD in its plane is used to account for the qualitative appearance of the spectrum. The form of the OH( $\nu=0$ ) and OH( $\nu=1$ ) torsional potentials which reproduce the qualitative features of the spectrum are slightly asymmetric, double-minimum potentials with large-amplitude excursions for HOD over nearly 180°. © 1995 American Institute of Physics.

## I. INTRODUCTION

The interaction between benzene and water has received much attention<sup>1-10</sup> as a prototype for the  $\pi$  hydrogen bond, i.e., the "hydrogen bond" formed when water's hydrogen(s) are donated to the delocalized  $\pi$  cloud of benzene. Spectroscopic studies of the gas phase C<sub>6</sub>H<sub>6</sub>–H<sub>2</sub>O complex<sup>2-6</sup> have recently added new insight to these interactions. Among the more important conclusions of these studies is that the C<sub>6</sub>H<sub>6</sub>–H<sub>2</sub>O intermolecular potential supports large-amplitude tumbling of water about benzene's surface already at the zero point level.<sup>2-4</sup> This ability of water to reorient on the aromatic  $\pi$  cloud with little cost in energy is qualitatively different than the more traditional, linear Y...H–X hydrogen bond with a localized electron pair.

Since the H–X stretching mode vibrates directly against the hydrogen bond, its infrared absorption provides a sensitive probe of the hydrogen bond.<sup>11,12</sup> Typical effects of the hydrogen bond include a red-shift in the H–X stretch frequency, an increase in the H–X absorption strength, and a broadening of its absorption. In the present paper, O–H stretch infrared spectra of the C<sub>6</sub>H<sub>6</sub>–H<sub>2</sub>O and C<sub>6</sub>H<sub>6</sub>–HOD complexes are reported and analyzed with the intent of further probing this prototypical  $\pi$  hydrogen bond. We will see that the large-amplitude motions of H<sub>2</sub>O on benzene have profound effects on the OH stretch infrared spectra. Figure 1 presents a reference configuration for the C<sub>6</sub>H<sub>6</sub>–H<sub>2</sub>O complex in which the relevant internal rotation/torsion angular coordinates ( $\phi$ ,  $\rho$ , and  $\chi$ ) of H<sub>2</sub>O are defined.

The matrix isolation study of Engdahl and Neland<sup>1</sup> provided the first evidence for nonrigidity in the complex, concluding that the C<sub>6</sub>H<sub>6</sub>–H<sub>2</sub>O complex has effective C<sub>6</sub> symmetry and that the two hydrogens of H<sub>2</sub>O are equivalent. In the gas phase complex, resonant two-photon ionization (R2PI) spectra<sup>2</sup> of C<sub>6</sub>H<sub>6</sub>–H<sub>2</sub>O and C<sub>6</sub>H<sub>6</sub>–D<sub>2</sub>O established that the vibrationally averaged position for the water molecule is on benzene's sixfold axis with a center-of-mass separation of 3.32±0.07 Å. Consistent with the matrix isolation data, vibronic symmetry arguments and the molecule's S<sub>0</sub>–S<sub>1</sub> rotational band contour have shown that the water molecule is capable of internal rotation which (i) retains an effective sixfold symmetry for the complex and (ii) occurs via exchange of water's hydrogens. The analysis of the spectra<sup>2</sup> was carried out in the framework of the G<sub>24</sub> molecular symmetry group in which H–H exchange on H<sub>2</sub>O is feasible.

The fourier transform microwave spectra of Suzuki *et al.*<sup>3</sup> and Gutowsky *et al.*<sup>4</sup> confirm and sharpen this picture. Rotational transitions out of the lowest energy levels of C<sub>6</sub>H<sub>6</sub>–H<sub>2</sub>O and C<sub>6</sub>H<sub>6</sub>–D<sub>2</sub>O ( $m=0$ ,  $\Sigma$  and  $m=1$ ,  $\Pi$ ) are those of a symmetric top, for which internal rotation about benzene's sixfold axis (angular coordinate  $\phi$ ) must be free or nearly free. The best-fit rotational constants provide a much more accurate center-of-mass separation between C<sub>6</sub>H<sub>6</sub> and H<sub>2</sub>O (3.329 Å). It was determined that the hydrogens of water are oriented preferentially toward the ring, i.e., in a  $\pi$  hydrogen-bonding configuration.

Computational studies of the C<sub>6</sub>H<sub>6</sub>–H<sub>2</sub>O complex reproduce the nearly free one-dimensional internal rotation of the

<sup>a)</sup> Author to whom correspondence should be addressed.

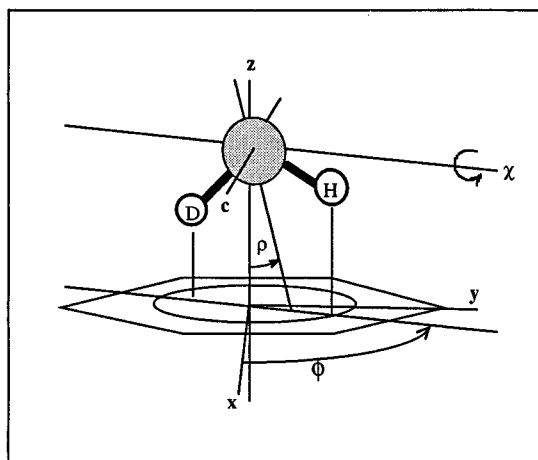


FIG. 1. Reference configuration for the C<sub>6</sub>H<sub>6</sub>-H<sub>2</sub>O and C<sub>6</sub>H<sub>6</sub>-HOD complexes with the three internal rotation/torsional angular coordinates defined.  $\phi$  is the internal rotation angle about the sixfold axis of benzene.  $\rho$  is the rotation of H<sub>2</sub>O (HOD) about its  $c$  axis with  $\rho=0$  defined as the symmetric configuration in which the C<sub>2</sub> axis of H<sub>2</sub>O coincides with the C<sub>6</sub> axis of benzene.  $\chi$  is the out-of-plane torsional angle of the H<sub>2</sub>O molecule about an axis perpendicular to the  $c$  axis of H<sub>2</sub>O (HOD).

water molecule.<sup>3,7,8</sup> In addition, they predict a potential for torsion in the plane of the water molecule (angular coordinate  $\rho$ ) which is nearly flat over orientational changes of  $\pm 50^\circ$ . The highest level *ab initio* calculations<sup>3,13</sup> and calculations employing molecular mechanics on clusters (MMC) (Ref. 8) predict a global minimum for the complex in which one hydrogen is preferentially pointing toward benzene's  $\pi$  cloud ( $\rho=25^\circ-50^\circ$ ). The double minimum potential then possesses a small barrier ( $20-50\text{ cm}^{-1}$ ) at the  $\rho=0^\circ$  orientation in which water's hydrogens point symmetrically toward the ring. The other torsional coordinate ( $\chi$ ) is predicted to be much stiffer, with the most recent *ab initio* calculations<sup>3,13</sup> predicting a vibrational frequency of  $260\text{ cm}^{-1}$ .

Despite these detailed studies, quantitative experimental determination of the C<sub>6</sub>H<sub>6</sub>-H<sub>2</sub>O intermolecular potential is still lacking because the absolute energies of the intermolecular vibrations and internal rotations of the complex are not known. Equally unsettling, the recent microwave data and analysis of Gutowsky *et al.*<sup>4</sup> for several isotopes of C<sub>6</sub>H<sub>6</sub>-H<sub>2</sub>O has reopened the possibility that the best first-order model of water's motion on benzene may be a three-dimensional free internal rotor rather than the one-dimensional internal rotor inferred by the earlier studies.<sup>2,3</sup>

Recently, we reported resonant ion-dip infrared spectra (RIDIRS) of C<sub>6</sub>H<sub>6</sub>-(H<sub>2</sub>O)<sub>*n*</sub> with  $n=1-7$  in the OH stretch region.<sup>14,15</sup> At that time, only the general features of the C<sub>6</sub>H<sub>6</sub>-H<sub>2</sub>O spectrum were described, and no assignments were given. The present paper provides a more detailed set of data on C<sub>6</sub>H<sub>6</sub>-H<sub>2</sub>O, extends that data to include C<sub>6</sub>H<sub>6</sub>-HOD, and presents a semiquantitative analysis of the spectra. The large-amplitude motions (LAMs) present in these complexes produce a number of transitions which would be negligibly weak in the absence of LAM. We will see that in C<sub>6</sub>H<sub>6</sub>-HOD, the normally weak OH stretch/torsion combination band actually exceeds the intensity of

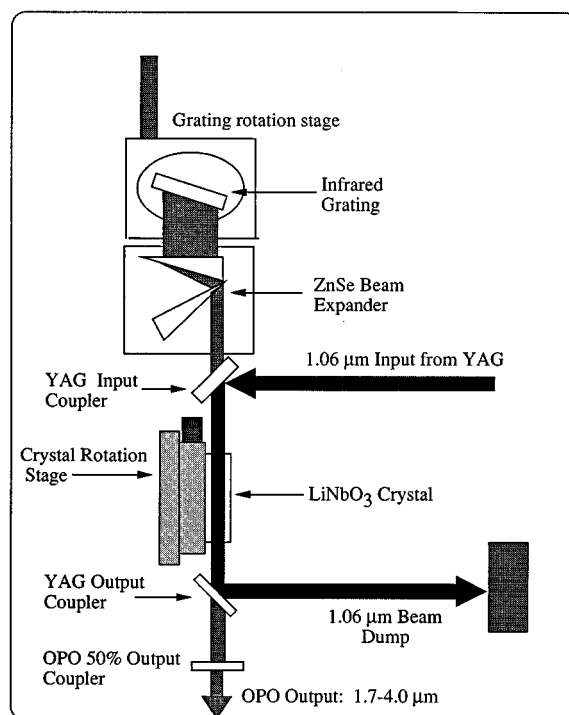


FIG. 2. Schematic diagram of the LiNbO<sub>3</sub> optical parametric oscillator used in the present study.

the OH stretch fundamental, a highly unusual occurrence in infrared spectroscopy. Our analysis points to two LAMs of significant consequence in the complexes; internal rotation about the sixfold axis of benzene ( $\phi$ ) and torsion along  $\rho$ .

## II. EXPERIMENT

Resonant ion-dip infrared spectra in the OH stretch region are recorded using methods described previously.<sup>14,15</sup> Details of the optical parametric oscillator (OPO), which have not been provided elsewhere, are given here. Briefly, cold, gas-phase C<sub>6</sub>H<sub>6</sub>-H<sub>2</sub>O and C<sub>6</sub>H<sub>6</sub>-HOD complexes are formed in a pulsed supersonic expansion. The complexes are interrogated in the ion-source region of a time-of-flight mass spectrometer (TOFMS), approximately 15 cm from the pulsed nozzle. The complex of interest is singled out for study using resonant two-photon ionization (R2PI) through its  $S_0-S_1$   $6_0^1$  transition. The ultraviolet laser (0.1–0.5 mJ/pulse) used for R2PI traverses twice through the ion source region of the TOFMS in a collimated beam of 1 mm diam. The ions from the two passes are born at slightly different potentials in the ion source, and arrive at the microchannel plate ion detector as two ion packets separated by about 200 ns. The arrival times of the ion mass of interest (C<sub>6</sub>H<sub>6</sub>-H<sub>2</sub>O or C<sub>6</sub>H<sub>6</sub>-HOD) are monitored with a digital oscilloscope.

A LiNbO<sub>3</sub> infrared optical parametric oscillator (OPO), shown schematically in Fig. 2, is used to produce the pulsed, tunable infrared radiation for the experiment. The fundamental output ( $1.064\text{ }\mu\text{m}$ ) of an unseeded Nd:YAG laser is propagated to the far field (20 m) and collimated to a beam diameter of 6 mm before entry into the OPO. Typical  $1.06\text{ }\mu\text{m}$  input powers at the OPO are 250 mJ/pulse in a 12 ns

pulse (achieved by delaying the Nd:YAG  $Q$ -switch). The YAG fundamental is single-passed through a  $10 \times 10 \times 50$  mm LiNbO<sub>3</sub> crystal mounted in an optical cavity which resonates the signal beam ( $1.45$ – $2.1 \mu\text{m}$ ). An infrared grating (600 lines/mm blazed at  $1.6 \mu\text{m}$ ) and ZnSe beam expander (X5) achieve  $\sim 1.5 \text{ cm}^{-1}$  resolution as measured in a photoacoustic spectrum of methane or H<sub>2</sub>O. Total output powers are typically 10–25 mJ/pulse, split approximately 3:1 between signal and idler beams. Wavelength scans are achieved by computer control of rotation stages on which the LiNbO<sub>3</sub> crystal and infrared grating are mounted. A calibration file for the OPO is generated over the wavelength range of interest using an infrared photodiode to view a reflection from the idler beam. Over the wavelength range of interest here, the absolute OPO wavelength is determined against known transitions in the infrared spectrum of water vapor, recorded using the photoacoustic signal produced by water vapor in the air.

The OPO output is collimated and loosely focused to the center of the ion source region of the TOFMS, where it is overlapped with one of the two passes of the ultraviolet laser used for R2PI. The OPO laser pulse typically precedes the R2PI laser by 100–500 ns. When an infrared absorption occurs out of the same ground-state level as that monitored in R2PI, a decrease in ion signal from the overlapped R2PI beam is observed. With normalization of the two ion signals, the percent depletion in ion signal is monitored as a function of OPO wavelength. The dual-beam method removes a major source of noise in the depletion experiment arising from shot-to-shot power fluctuations in the R2PI laser.

C<sub>6</sub>H<sub>6</sub>-H<sub>2</sub>O complexes are formed from a gas mixture containing 0.1% benzene and 0.2%–0.4% H<sub>2</sub>O in helium at a backing pressure of 4 bar. C<sub>6</sub>H<sub>6</sub>-HOD complexes were made from a 50–50 H<sub>2</sub>O/D<sub>2</sub>O mixture.

### III. RESULTS

The RIDIR spectrum of C<sub>6</sub>H<sub>6</sub>-H<sub>2</sub>O in the OH stretch region is shown in Fig. 3(a). The nonrigidity of the complex is immediately obvious from the spectrum. In a rigid complex with a single, well-defined structure, the OH stretch infrared spectrum should be comprised of two transitions rather than the seven or more transitions observed.

The spectrum of Fig. 3(a) was recorded by monitoring the parent ion mass with the R2PI laser tuned to the peak maximum of the  $6_0^1$  transition of the complex, shown in Fig. 3(b). We have shown previously<sup>2</sup> that this band of C<sub>6</sub>H<sub>6</sub>-H<sub>2</sub>O is comprised of two partially overlapped  $\Delta m = 0$  transitions out of the  $m = 0$  ( $\Sigma$ ) and  $m = 1$  ( $\Pi$ ) levels of internally rotating C<sub>6</sub>H<sub>6</sub>-H<sub>2</sub>O. Due to the different nuclear spin symmetries of H<sub>2</sub>O in these levels (para and ortho, respectively), collisional cooling in the expansion<sup>2</sup> does not convert between these lowest two levels, so that C<sub>6</sub>H<sub>6</sub>-H<sub>2</sub>O complexes are present in the expansion in both  $\Sigma$  and  $\Pi$  ground state levels, giving rise to the partially resolved transitions in the R2PI spectrum. As a result, the RIDIR spectrum of Fig. 3(a) also contains transitions out of both  $\Sigma$  and  $\Pi$  ground state levels of the complex.

If the  $\Sigma$ - $\Sigma$  and  $\Pi$ - $\Pi$  transitions were completely resolved in R2PI, RIDIR spectra out of the two ground state

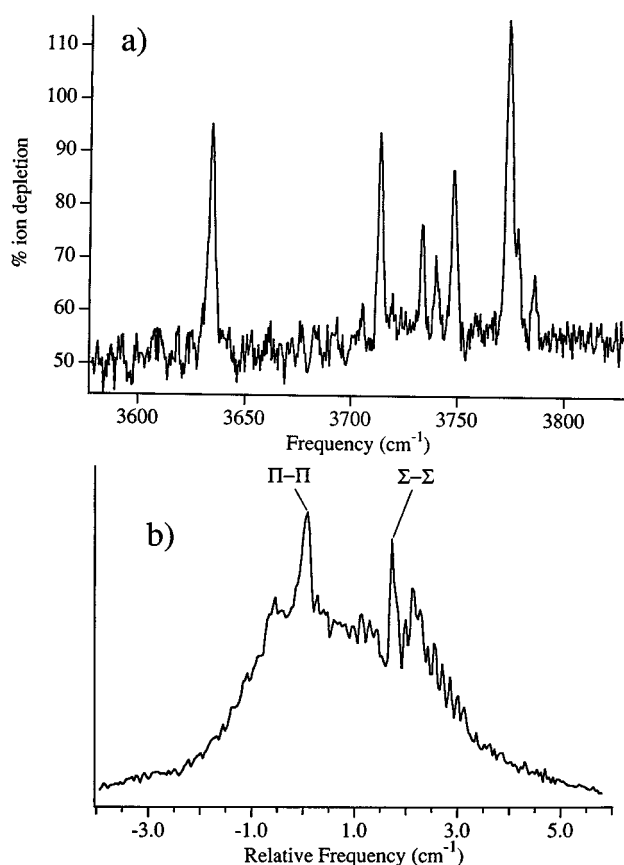


FIG. 3. (a) Resonant ion-dip infrared spectrum of the C<sub>6</sub>H<sub>6</sub>-H<sub>2</sub>O complex in the OH stretch region. (b) R2PI spectrum of the  $6_0^1$  transition of C<sub>6</sub>H<sub>6</sub>-H<sub>2</sub>O. In recording the RIDIR spectrum, the parent ion mass is monitored with the resonant two-photon ionization laser tuned to the peak of the partially overlapped  $\Pi$ - $\Pi$   $6_0^1$  transition in C<sub>6</sub>H<sub>6</sub>-H<sub>2</sub>O shown by an arrow.

levels could be recorded free from interference from one another. This is one of the potential strengths of RIDIR spectroscopy; namely, its ability to record infrared spectra of different conformers or vibrational levels of the same mass. However, the R2PI laser power required to obtain adequate ion signal for the RIDIR spectra leads to power broadening of the R2PI transitions. When combined with the partial overlap of the bands, it has not been possible to record infrared spectra from the  $\Sigma$  and  $\Pi$  ground state levels free from interference. However, Figs. 4(a) and 4(b) show two spectra recorded with R2PI laser tuned to the maximum of the  $\Sigma$ - $\Sigma$  and  $\Pi$ - $\Pi$   $6_0^1$  transitions, respectively. A comparison of these spectra indicates that the transitions labeled  $\Pi_{\text{gs}}$  and  $\Sigma_{\text{gs}}$  arise out of the  $\Pi(m = 1)$  and  $\Sigma(m = 0)$  ground state levels, respectively. At the present signal to noise, the other transitions are less clearly assigned in this way.

Figure 5(a) displays the RIDIR spectra of C<sub>6</sub>H<sub>6</sub>-HOD in the OH stretch region while monitoring the complex's  $6_0^1$  transition in R2PI [shown in Fig. 5(b)]. The isotopic substitution removes the nuclear spin distinction between  $m = 0$  and  $m = 1$  levels, allowing cooling between them. In the free HOD molecule, the OH stretch region of the infrared contains a single transition at  $3707 \text{ cm}^{-1}$ . This vibration is essentially a local mode stretch along the OH bond. By con-

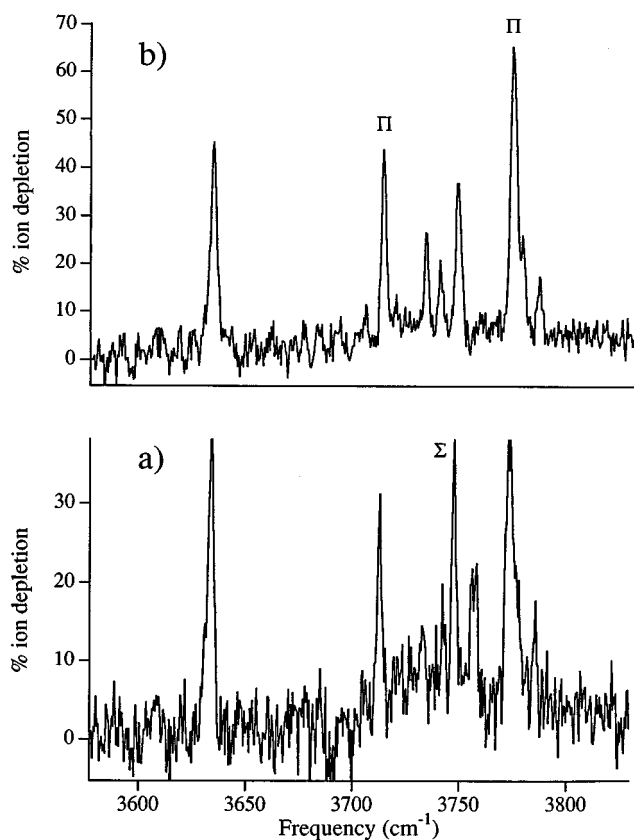


FIG. 4. RIDIR spectra of C<sub>6</sub>H<sub>6</sub>-H<sub>2</sub>O with R2PI laser tuned to the peak of the (a)  $\Sigma$ - $\Sigma$  and (b)  $\Pi$ - $\Pi$   $6_0^1$  transitions of the complex. Power saturation and partial overlap of the bands prevents complete separation of the two spectra. However, a comparison of the two spectra provides an assignment of the labeled transitions as arising from the  $\Pi$  ground state.

trast, the OH stretch region of C<sub>6</sub>H<sub>6</sub>-HOD is composed of five transitions spread over 50 cm<sup>-1</sup>. Initially, it was thought that some of these transitions might be due to hot bands which were unresolved in the R2PI transition being monitored. However, the RIDIR spectrum is unchanged with changing position in the R2PI band contour or by drastic changes in the cooling in the expansion. In fact, at the lowest backing pressures, a hot band grew in the R2PI spectrum. The RIDIR spectrum out of the ground state level responsible for this R2PI hot band was indistinguishable from the  $6_0^1$  transition. We conclude that the structure observed in the C<sub>6</sub>H<sub>6</sub>-HOD RIDIR spectrum arises entirely from the zero point level of the complex. Low frequency combination bands built on the OH stretch must then be responsible for the additional transitions observed, and these are much more intense than the fundamental.

#### IV. ANALYSIS

The transitions observed for C<sub>6</sub>H<sub>6</sub>-H<sub>2</sub>O span the frequency range from 3634 to 3782 cm<sup>-1</sup>. These fall generally into two clumps; a single transition at 3634 cm<sup>-1</sup>, and a set of transitions with center-of-gravity about 3740 cm<sup>-1</sup>. Felker and co-workers<sup>6</sup> have recently recorded ionization loss stimulated Raman spectra of C<sub>6</sub>H<sub>6</sub>-H<sub>2</sub>O in the OH stretch region. They find a single transition at 3634 cm<sup>-1</sup> which they

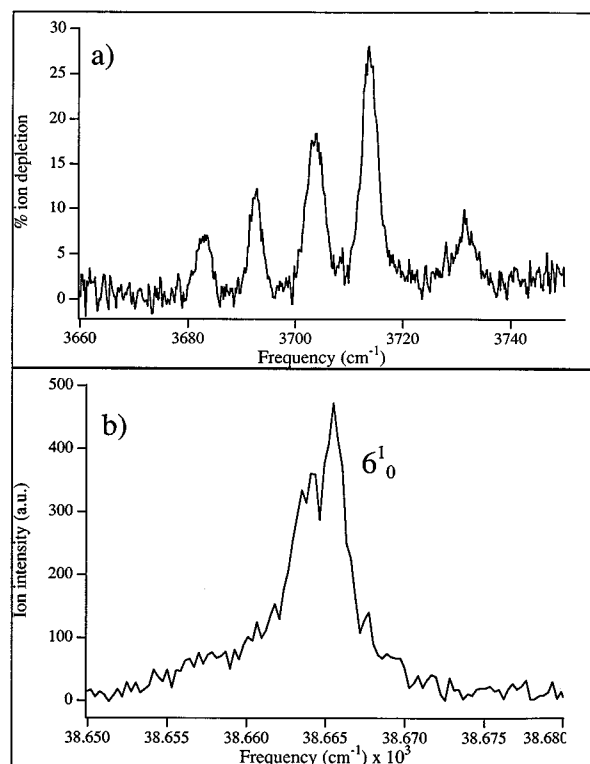


FIG. 5. (a) Resonant ion-dip infrared spectrum of the C<sub>6</sub>H<sub>6</sub>-HOD complex in the OH stretch region. (b) R2PI spectrum of the  $6_0^1$  transition of C<sub>6</sub>H<sub>6</sub>-HOD. In recording the RIDIR spectrum, the parent ion mass is monitored with the R2PI laser tuned to the peak of the  $6_0^1$  transition.

assign to the symmetric stretch of H<sub>2</sub>O in the complex. This is quite reasonable given the small frequency shift (23 cm<sup>-1</sup>) from the symmetric stretch in free H<sub>2</sub>O. None of the transitions observed above 3700 cm<sup>-1</sup> in the infrared are detected in the Raman spectrum due to the much weaker Raman activity of the asymmetric stretch. This argues for treatment of the OH stretch transitions as symmetric and antisymmetric stretch rather than as local mode OH stretches. As we will see, analysis based on symmetric and antisymmetric stretch modes predicts  $\nu_3^0$  at about 3731 cm<sup>-1</sup>, giving a frequency difference of 97 cm<sup>-1</sup> between symmetric and antisymmetric stretches, i.e., within a few wave numbers of that in free H<sub>2</sub>O (99 cm<sup>-1</sup>). The transitions can therefore be regarded as nominally symmetric and antisymmetric stretch transitions, since even a modest force constant difference between the two OH bonds in C<sub>6</sub>H<sub>6</sub>-H<sub>2</sub>O would produce a frequency difference significantly greater than 100 cm<sup>-1</sup>.<sup>16</sup> For instance, in the water dimer,<sup>17</sup> the free OH and H-bonded OH of the donor H<sub>2</sub>O molecule have a frequency difference of 176 cm<sup>-1</sup>.

#### A. The nature of the large-amplitude motions in C<sub>6</sub>H<sub>6</sub>-H<sub>2</sub>O and C<sub>6</sub>H<sub>6</sub>-HOD

In considering the most appropriate model for analyzing the spectra of C<sub>6</sub>H<sub>6</sub>-H<sub>2</sub>O and C<sub>6</sub>H<sub>6</sub>-HOD, it is worth setting down the predictions of various limiting cases, restricting our attention for the moment to C<sub>6</sub>H<sub>6</sub>-H<sub>2</sub>O.

### 1. H<sub>2</sub>O rigidly held to C<sub>6</sub>H<sub>6</sub>

If C<sub>6</sub>H<sub>6</sub>-H<sub>2</sub>O were a rigid complex, only two transitions should be observed in the OH stretch region (sym/asym stretch or free/ $\pi$  H-bond OH), counter to observation. A rigid complex is also at odds with the R2PI and microwave data which show C<sub>6</sub>H<sub>6</sub>-H<sub>2</sub>O to be a symmetric top.<sup>2-4</sup>

### 2. Nearly free three-dimensional (3D) internal rotation of H<sub>2</sub>O

At the other extreme from a rigid complex is one in which water undergoes nearly free three-dimensional internal rotation about its equilibrium position on benzene. This is the possibility raised by Gutowsky *et al.*<sup>4</sup> for C<sub>6</sub>H<sub>6</sub>-H<sub>2</sub>O based primarily on the nuclear spin hyperfine splittings observed for  $m=0$  and  $m=1$ .

The Ar-H<sub>2</sub>O complex is a prototype for this behavior.<sup>18-20</sup> Not unexpectedly, the small binding energy of argon to H<sub>2</sub>O produces only weak perturbations on free water's rotational levels and wave functions. In Ar-H<sub>2</sub>O, the small anisotropy in the potential breaks the  $(2j+1)$ -fold degeneracy of an internally rotating H<sub>2</sub>O in level  $j_{k_1 k_2 k_3}$ , but the center-of-gravity of the split levels is near to that of the corresponding level of free H<sub>2</sub>O. The  $0_{00}$  level of free H<sub>2</sub>O is nondegenerate and has para nuclear spin symmetry. The lowest ortho level of Ar-H<sub>2</sub>O correlates with  $1_{01}$ , which splits into  $\Sigma(1_{01})$  and  $\Pi(1_{01})$  levels. The lower of these in Ar-H<sub>2</sub>O is  $\Sigma(1_{01})$ , and transitions are observed primarily out of the lowest para and ortho levels of the complex,  $\Sigma(0_{00})$  and  $\Sigma(1_{01})$ , respectively. Lascola and Nesbitt<sup>20</sup> have recorded fully rotationally resolved spectra of four transitions in the antisymmetric stretch region. No transitions have been reported in the symmetric stretch region due to its weaker intensity.

The prediction of this model for C<sub>6</sub>H<sub>6</sub>-H<sub>2</sub>O, irrespective of the relative ordering of  $\Sigma(1_{01})$  and  $\Pi(1_{01})$ , is that the symmetric stretch region (like the asymmetric stretch region) should be comprised of several transitions of similar intensity rather than the single transition observed in both Raman<sup>6</sup> and infrared spectra (Fig. 3). This suggests that a nearly free 3D rotation of H<sub>2</sub>O in the complex is not the most appropriate first-order picture for water's internal motion on benzene.

### 3. Free one-dimensional (1D) internal rotation of H<sub>2</sub>O

In this model, the water molecule can internally rotate about benzene's sixfold axis nearly freely, but has significant anisotropy for rotation about axes perpendicular to the sixfold axis. Here, the 1D internal rotor levels will have energies given by

$$E = B \cdot m^2, \text{ where } m = 0, \pm 1, \pm 2, \dots$$

At the same time, if the energy difference between hydrogens down and oxygen down is large enough, the energy levels for the other hindered internal rotations at low energies can be approximated as torsional vibrations.

Both R2PI (Ref. 2) and microwave<sup>3,4</sup> spectra show that C<sub>6</sub>H<sub>6</sub>-H<sub>2</sub>O is a symmetric top, consistent with free internal rotation of H<sub>2</sub>O relative to benzene. Confirmation for this model can be drawn from recent *ab initio*<sup>3,13</sup> and MMC (Ref.

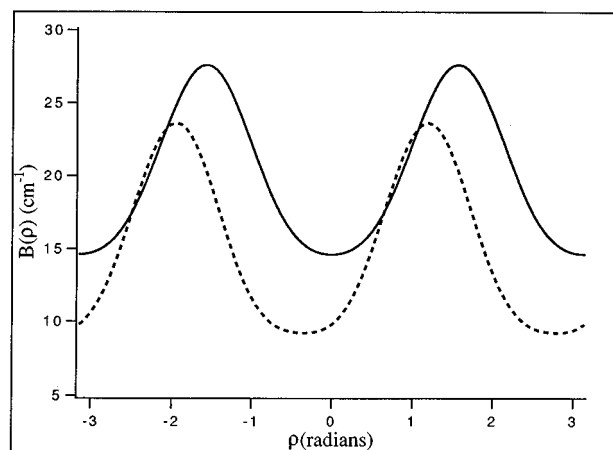


FIG. 6. Internal rotation constant, in wave numbers, for motion in  $\phi$  (i.e., about the sixfold axis of benzene) as a function of angle  $\rho$ . —, C<sub>6</sub>H<sub>6</sub>-H<sub>2</sub>O; ---, C<sub>6</sub>H<sub>6</sub>-HOD.

8) calculations of C<sub>6</sub>H<sub>6</sub>-H<sub>2</sub>O. In the MMC potential,<sup>21</sup> the anisotropy in the potential (H down vs O down) is calculated to be about 200 cm<sup>-1</sup>, supporting the treatment of the lowest hindered rotor levels along  $\rho$  and  $\chi$  (Fig. 1) as torsional vibrations. The 1D internal rotation, on the other hand, is essentially free with internal rotation constant calculated as  $B \sim 16$  cm<sup>-1</sup> (Fig. 6).

The recent high-level *ab initio* results of Suzuki *et al.*<sup>3</sup> also predicts both free 1D internal rotation about benzene's sixfold axis and significant anisotropy in other dimensions. Torsional vibrational frequencies along  $\rho$  and  $\chi$  are calculated to be 47 and 260 cm<sup>-1</sup>, respectively.

In order to assess the major features of the OH stretch infrared spectrum predicted by this model, the rovibrational selection rules<sup>22</sup> for symmetric and antisymmetric stretch will be those of a symmetric top undergoing free internal rotation about the top axis. As a parallel band, the symmetric stretch will have

$$\Delta v_1 = \pm 1, \quad \Delta K = 0, \quad \text{and} \quad \Delta m = 0, \quad (1)$$

where  $v$  is the vibrational quantum number,  $K$  is the projection of the total angular momentum along the top axis, and  $m$  is the internal rotation quantum number. Similarly, the asymmetric stretch, as a perpendicular band, will have

$$\Delta v_3 = \pm 1, \quad \Delta K = \pm 1, \quad \text{and} \quad \Delta m = \pm 1. \quad (2)$$

The lowest para and ortho levels of the complex are the  $m=0$  ( $\Sigma$ ) and  $m=1$  ( $\Pi$ ) internal rotor levels, respectively, and infrared transitions should be present out of both of these. Thus, in the limit of free 1D internal rotation, the symmetric stretch transition should be composed of two parallel subbands at the indicated frequencies

$$\Sigma - \Sigma \quad \text{at } \nu_1^0$$

and

$$\Pi - \Pi \quad \text{at } \nu_1^0 + (B'_s - B''),$$

where  $B'_s$  is the internal rotor constant for the  $v=1$  level of the symmetric stretch. If, as expected,  $(B'_s - B'')$  is small,

the two bands will be unresolved, and a single transition should appear in the symmetric stretch region.

For the asymmetric stretch, three perpendicular transitions should appear:

$$\Sigma-\Pi \quad \text{at } \nu_3^0 + B'_a,$$

$$\Pi-\Sigma \quad \text{at } \nu_3^0 - B'',$$

and

$$\Pi-\Delta \quad \text{at } \nu_3^0 + 4B'_a - B'',$$

where  $B'_a$  is the internal rotor constant for the  $\nu=1$  level of the antisymmetric stretch. If  $B'_a = B''$ , the three transitions will be equally spaced with separation  $2B''$ .

Comparison of the experimental spectrum with these predictions is encouraging. We assign the  $3634 \text{ cm}^{-1}$  transition as the unresolved  $\Sigma-\Sigma$  and  $\Pi-\Pi$  parallel bands of the symmetric stretch. The three dominant transitions in the asymmetric stretch region are at  $3713$ ,  $3748$ , and  $3774 \text{ cm}^{-1}$ , which we assign as the  $\Pi-\Sigma$ ,  $\Sigma-\Pi$ , and  $\Pi-\Delta$  transitions, respectively. Of course, these transitions are not equally spaced. Within the confines of a free 1D internal rotation model, we would need to conjecture unequal internal rotation constants in the ground and vibrationally excited states, i.e.,  $B'' \approx 20 \text{ cm}^{-1}$  and  $B'_a \approx 15 \text{ cm}^{-1}$ . However, other features of the spectra call for the need for refinement of the 1D model.

#### 4. 2D large-amplitude motion along $\phi$ and $\rho$

While the general features of the spectrum of C<sub>6</sub>H<sub>6</sub>-H<sub>2</sub>O are accounted for by 1D free internal rotation of H<sub>2</sub>O on benzene (along  $\phi$ ), other aspects of the spectra of Figs. 3 and 5 suggest the need for some modifications of the 1D model. First, the model does not account for the several weak transitions present in the asymmetric stretch region of C<sub>6</sub>H<sub>6</sub>-H<sub>2</sub>O, most notably at  $3733$ ,  $3739$ , and  $3782 \text{ cm}^{-1}$ .

Second, the C<sub>6</sub>H<sub>6</sub>-HOD spectrum of Fig. 5 is composed of five transitions out of a single ground state [the  $\Sigma(m=0)$  state], yet only two of these can be assigned via free 1D internal rotation alone. As stated before, the OH stretch transition in HOD is essentially a local-mode stretch along the OH bond. The vibrationally-averaged orientation of this bond in C<sub>6</sub>H<sub>6</sub>-HOD will produce a parallel ( $\Sigma-\Sigma$ ) and a perpendicular ( $\Sigma-\Pi$ ) transition; i.e.,

$$\Sigma-\Sigma \quad \text{at } \nu_{\text{OH}}^0,$$

$$\Sigma-\Pi \quad \text{at } \nu_{\text{OH}}^0 + B'_{\text{OH}},$$

where  $B'_{\text{OH}}$  is the internal rotation constant for HOD in the OH ( $\nu=1$ ) excited state. As experiment has shown (Sec. III), the corresponding transitions out of the  $\Pi$  ground state are not present because nuclear spin restrictions on cooling from  $\Pi$  to  $\Sigma$  have been removed by the isotopic substitution. Furthermore, even if they were present, the relative positions and intensities of the bands cannot be accounted for even qualitatively by their incorporation.

Instead, the 1D model must be refined to include a second large-amplitude motion; namely, the in-plane torsion of the water molecule along angle  $\rho$  (Fig. 1). Based on the *ab*

*initio* calculations, it is reasonable to suggest that the in-plane torsion be large-amplitude, since both *ab initio*<sup>3</sup> and MMC (Ref. 13) calculations on C<sub>6</sub>H<sub>6</sub>-H<sub>2</sub>O have predicted a broad, flat potential for H<sub>2</sub>O tumbling along  $\rho$  over angular changes of  $\pm 50^\circ$  or more, possibly with a small barrier present at  $\rho=0^\circ$ . Furthermore, torsion along  $\rho$  will change the orientation of the OH bonds, thereby inducing intensity in OH stretch/torsion combination bands.

In the next two sections, we will develop this model, apply it to C<sub>6</sub>H<sub>6</sub>-HOD first, before returning to C<sub>6</sub>H<sub>6</sub>-H<sub>2</sub>O for a final look at the model's consequences there. In C<sub>6</sub>H<sub>6</sub>-HOD, the goal of the modeling is to account for the presence of five resolved transitions out of a single ground state in which combination bands significantly exceed the intensity of the fundamental. C<sub>6</sub>H<sub>6</sub>-H<sub>2</sub>O will serve as a consistency check, and provide some added insight to the substantial differences between the spectra of the symmetric and asymmetric isotopes.

### B. A 2D ( $\rho, \phi$ ) LAM model of the OH stretch IR spectrum

#### 1. The model Hamiltonian

The form of the model Hamiltonian in  $\rho$  and  $\phi$  is

$$H = -\frac{\hbar^2}{2I_c} \left( \frac{\partial^2}{\partial \rho^2} \right) - F(\rho) \left( \frac{\partial^2}{\partial \phi^2} \right) + V(\rho), \quad (3)$$

where the coordinates  $\rho$  and  $\phi$  are defined in Fig. 1. The first term is the kinetic energy for motion along  $\rho$  (the  $c$  axis of water), the second term that for internal rotation about the sixfold axis of benzene (the  $z$  axis) with internal rotation constant  $F(\rho) = -[\hbar^2/2I_z(\rho)]$ , and  $V(\rho)$  is the intermolecular potential along  $\rho$  assuming  $V(\phi)=0$ . The Hamiltonian thus focuses attention on internal rotation of the H<sub>2</sub>O or HOD molecule in the potential produced by the benzene molecule. The angle  $\rho$  is not to be confused with either the spherical coordinate or the Euler angle  $\theta$  in that it takes on both positive and negative values (rather than a value in the range 0 to  $\pi$ ). Such a definition is useful for treatment of motion along  $\rho$  as a torsional vibration rather than a hindered internal rotation. Coupling to the torsion in  $\chi$ , the intermolecular bends or the intermolecular stretching modes is also ignored.

This simple Hamiltonian is solved for the torsion/internal rotation energy levels using a product basis of harmonic oscillator functions along  $\rho$  and free internal rotor functions in  $\phi$ ,

$$\psi_{vm}(y, \phi) = \left[ \sum_{n=0}^5 a_n N_n H_n(y) \exp(-y^2/2) \right] \exp(-im\phi), \quad (4)$$

where

$$y = 2\pi \left( \frac{\tilde{\nu}_i c}{h} \right)^{1/2} Q_{\text{tor}}, \quad (5)$$

and  $\tilde{\nu}_i$  is the harmonic torsional vib. freq. in  $\text{cm}^{-1}$ .

For HOD,  $Q_{\text{tor}} \approx (m_{\text{H}} + m_{\text{D}})^{1/2} r_0 \rho$ . With  $\rho$  in radians and  $\tilde{\nu}_i$  in wave numbers,  $y = 0.286 \nu_i^{1/2} \rho$  for HOD. For H<sub>2</sub>O,  $Q_{\text{tor}} \approx (2m_{\text{H}})^{1/2} r_0 \rho$  so that  $y = 0.233 \nu_i^{1/2} \rho$ .

## 2. The form of the effective potential

The zeroth order form of the torsional potential is assumed to be harmonic,

$$V_0(\rho) = \frac{1}{2}k\rho^2.$$

However, the effective potential can have deviations from this form arising from several sources; anharmonicity in the intermolecular potential, kinetic coupling to internal rotation about  $\phi$ , and  $\rho$ -dependent adiabatic zero point corrections from other vibrational modes, i.e.,

$$V_{\text{pert}}(\rho) = V_{\text{IM}}(\rho) + F(\rho)m^2 + V_{\text{ZP}}(\rho). \quad (6)$$

*a. Anharmonicity.* The anharmonicity in the intermolecular potential is anticipated based on the *ab initio*<sup>3</sup> and MMC (Ref. 13) calculations, which predict a double minimum well with small barrier at  $\rho=0^\circ$ . The excited state potential might also be expected to differ somewhat from the ground state potential due to the increased polarizability of the vibrationally excited state.

*b. Kinetic coupling to internal rotation in  $\phi$ .* Kinetic coupling to internal rotation about  $\phi$  is an obvious consequence of the sensitive dependence of the internal rotation constant  $F$  on the orientation  $\rho$  of HOD. The assumption of free internal rotation about  $\phi$  for all angles  $\rho$  insures that the  $\phi$  dependence of the wave function is given by  $\exp(-im\phi)$ . The Hamiltonian then block-diagonalizes into  $\Sigma(m=0)$ ,  $\Pi(m=\pm 1)$ ,  $\Delta(m=\pm 2)$ ,... states and the effective potential in  $\rho$  has added to it a centrifugal barrier term  $F(\rho)m^2$ . If torsion in  $\rho$  were small-amplitude about angle  $\rho_0$ , the centrifugal barrier term would be a constant  $[F(\rho_0)m^2]$  and the Hamiltonian would be separable in  $\rho$  and  $\phi$ .

For larger-amplitude motions along  $\rho$ , the varying internal rotation constant  $F(\rho)$  modulates the free internal rotor energy levels as shown in Fig. 6. The effect on the  $\rho$ -dependent potential is significant, modulating  $\Pi$  state potentials in C<sub>6</sub>H<sub>6</sub>-HOD by 14 cm<sup>-1</sup> (between 9.1 and 23.5 cm<sup>-1</sup>) and  $\Delta$  states by 4 times this. Note that  $F(\rho)$  is a symmetric function of  $\rho$  in H<sub>2</sub>O, but is distinctly asymmetric in HOD. This asymmetry arises from the rotation of the inertial axes in HOD by 21° relative to H<sub>2</sub>O, with the “*a*” axis rotated toward the OD bond. Thus, in C<sub>6</sub>H<sub>6</sub>-HOD, the  $\rho$ -dependent potential for the states with  $m>0$  (i.e.,  $\Pi, \Delta, \dots$ ) has this asymmetric component favoring the H down configurations over those with D down. In C<sub>6</sub>H<sub>6</sub>-H<sub>2</sub>O, the  $F(\rho) \cdot m^2$  term steepens the walls of the  $\rho$ -dependent potential about  $\rho=0^\circ$ .

If vibration in  $\rho$  and internal rotation in  $\phi$  occur on very different time scales, adiabatic separation of the two motions would be possible. In the present case, the close proximity of the bands in the C<sub>6</sub>H<sub>6</sub>-HOD spectrum indicate that the two time scales are similar. We thus include the  $\rho$  dependence of the internal rotation constant  $F(\rho)$  explicitly in  $V_{\text{eff}}(\rho)$ .

*c. Zero point corrections from other vibrations.* Finally, the form of the effective  $\rho$ -dependent potential is also influenced by adiabatic zero point corrections from other vibrational coordinates. In C<sub>6</sub>H<sub>6</sub>-HOD, such adiabatic corrections to the intermolecular potential are responsible for the asymmetry in the ground state HOD potential reported by Gu-

towsky *et al.*<sup>4</sup> in which the vibrationally-averaged orientation for HOD is rotated 18° toward the D down configuration. One significant contribution to  $\rho$ -dependent zero point effects arises from the H<sub>2</sub>O and HOD OH(D) intramolecular stretch vibrations themselves. One would expect that, as H<sub>2</sub>O rotates along  $\rho$ , the strength of interaction of a given O-H bond with the benzene ring will change, thereby modifying the O-H stretch frequencies in a  $\rho$ -dependent fashion. Experimental evidence for this fact can be found in the larger C<sub>6</sub>H<sub>6</sub>-(H<sub>2</sub>O)<sub>*n*</sub> clusters<sup>14,15</sup> with  $n=3-5$  which possess a characteristic absorption due to  $\pi$  hydrogen-bonded OH which is red-shifted from the free OH stretch by about 60 cm<sup>-1</sup>. On the other hand, using the phenol-H<sub>2</sub>O complex<sup>23</sup> as a guide (where the H<sub>2</sub>O molecule accepts a hydrogen bond), the OH stretch vibrational frequencies should be changed only slightly ( $\sim 5$  cm<sup>-1</sup>) by the interaction with benzene in the oxygen down ( $\rho=180^\circ$ ) orientation.

In C<sub>6</sub>H<sub>6</sub>-HOD, the OH and OD stretches are local mode vibrations. The adiabatic correction from the OH/OD stretching modes is then

$$\frac{1}{2}\nu_{\text{OH}}(\rho) + \frac{1}{2}\nu_{\text{OD}}(\rho)$$

in the ground state, while in the OH and OD stretch excited state, it becomes

$$\frac{3}{2}\nu_{\text{OH}}(\rho) + \frac{1}{2}\nu_{\text{OD}}(\rho)$$

and

$$\frac{1}{2}\nu_{\text{OH}}(\rho) + \frac{3}{2}\nu_{\text{OD}}(\rho),$$

respectively. One expects that the maximum effect of benzene on the OH(OD) stretch should occur at  $\rho=-52^\circ(+52^\circ)$ , with OH (OD) pointing directly toward the ring. The  $\rho$ -dependent correction should be negligibly small near  $\rho=180^\circ$  (oxygen down) while at  $\rho=0^\circ$  it will be somewhere in between. Due to the compensating effects of OH and OD stretch modes, the ground state should have little additional asymmetry from these zero point corrections. However, the OH stretch contribution to  $V_{\text{eff}}(\rho)$  will favor OH(OD) down orientations in the OH(OD) ( $v=1$ ) excited states.

In C<sub>6</sub>H<sub>6</sub>-H<sub>2</sub>O, the nominally symmetric and asymmetric stretch modes are delocalized over both OH bonds. However, just as with OH and OD stretches in C<sub>6</sub>H<sub>6</sub>-HOD, the symmetric and asymmetric stretch vibrations may have different  $\rho$  dependencies. In the ground state, the zero point correction is

$$\frac{1}{2}\nu_1(\rho) + \frac{1}{2}\nu_3(\rho)$$

which in the symmetric and asymmetric stretch excited states become

$$\frac{3}{2}\nu_1(\rho) + \frac{1}{2}\nu_3(\rho)$$

and

$$\frac{1}{2}\nu_1(\rho) + \frac{3}{2}\nu_3(\rho),$$

respectively. It is important to note that these correction terms will likely be different than those in HOD. Thus, the

form of  $V_{\text{eff}}(\rho)$  cannot be expected to transfer without change between C<sub>6</sub>H<sub>6</sub>-HOD, C<sub>6</sub>H<sub>6</sub>-H<sub>2</sub>O symmetric stretch, and C<sub>6</sub>H<sub>6</sub>-H<sub>2</sub>O asymmetric stretch.

Thus, the contributions to  $V_{\text{pert}}(\rho)$  are from anharmonicities in the intermolecular potential, the  $\rho$ -dependent zero point level effects from other vibrations, and the centrifugal term due to internal rotation about  $\phi$ . In the modeling,  $V_{\text{pert}}(\rho)$  incorporates a double minimum well centered on  $\rho=0^\circ$  which goes asymptotically to zero at  $\rho=\pm 180^\circ$ . The height and width of the barrier at  $\rho=0^\circ$  can be varied, either with (HOD) or without (H<sub>2</sub>O) asymmetry.

### 3. $Q_1/Q_3$ mixing in C<sub>6</sub>H<sub>6</sub>-H<sub>2</sub>O as a function of $\rho$

In Sec. IV A 3, the 1D internal rotation model led to the deduction that the OH stretch modes in C<sub>6</sub>H<sub>6</sub>-H<sub>2</sub>O were nominally symmetric and asymmetric stretch based on  $(\nu_3^0 - \nu_1^0) \approx 100 \text{ cm}^{-1}$ . However, in recognizing the need for refinement of this model to include large-amplitude motion along  $\rho$ , one must also admit the possibility that some degree of dynamical localization of the OH stretch vibrations may occur. As the H<sub>2</sub>O molecule executes large-amplitude motion away from the symmetric  $\rho=0^\circ$  position, the two OH bonds become inequivalent by virtue of the different strength of their interaction with the benzene  $\pi$  cloud. In the limit of a very strong  $\pi$  hydrogen bond at the  $\rho=\pm 52^\circ$  orientations, the symmetric and asymmetric stretch modes would be turned into local mode OH stretches on the  $\pi$  hydrogen bonded and free OH's. Put another way, the interaction with benzene could lead to some mixing of the symmetric ( $Q_1$ ) and asymmetric stretch ( $Q_3$ ) modes as a function of  $\rho$ . Given the close proximity of the  $\nu=1$  OH stretch modes (split by  $100 \text{ cm}^{-1}$ ), the major effect of such mixing will be on the vibrationally excited states.

This mixing gains importance from the fact that the asymmetric stretch is twenty times more intense than the symmetric stretch.<sup>24,25</sup> Consequently, even a small amount of  $Q_1/Q_3$  mixing can have significant effects on intensities of combination bands, especially in the  $Q_1$  region. On the other hand, in C<sub>6</sub>H<sub>6</sub>-HOD, the corresponding modes are local mode OH and OD stretches split by  $1000 \text{ cm}^{-1}$  which will thereby be negligibly mixed as a function of angle  $\rho$ .

The effect of  $Q_1/Q_3$  mixing in C<sub>6</sub>H<sub>6</sub>-H<sub>2</sub>O can be modeled as follows. The unperturbed symmetric and asymmetric stretch modes are of the form

$$\text{symmetric stretch: } Q_1^0 = (1/2)^{1/2}(S_a + S_b), \quad (7)$$

$$\text{asymmetric stretch: } Q_3^0 = (1/2)^{1/2}(-S_a + S_b), \quad (8)$$

where  $S_a$  and  $S_b$  are the internal OH<sub>a</sub> and OH<sub>b</sub> coordinates.

The  $\rho$ -dependent mixing gives rise to normal coordinates which depend on  $\rho$ ,

$$Q_1(\rho) = \alpha(\rho)Q_1^0 + \beta(\rho)Q_3^0, \quad (9)$$

$$Q_3(\rho) = -\beta(\rho)Q_1^0 + \alpha(\rho)Q_3^0, \quad (10)$$

where  $\alpha(\rho)$  and  $\beta(\rho)$  are the normalized,  $\rho$ -dependent mixing coefficients.

In the vibrationally excited states, the wave functions are also  $\rho$ -dependent,

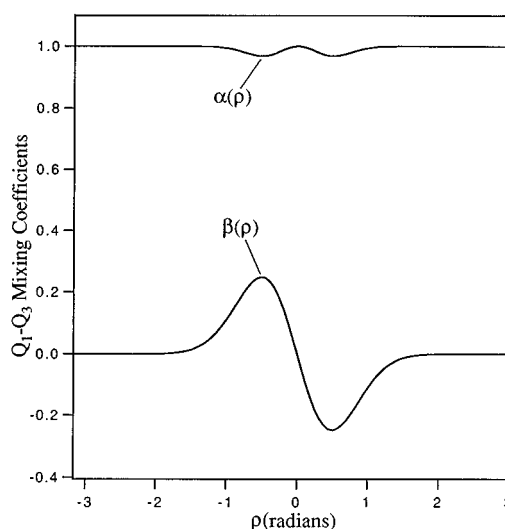


FIG. 7. The general functional form for  $\alpha(\rho)$  and  $\beta(\rho)$ , the symmetric stretch ( $Q_1$ )-asymmetric stretch ( $Q_3$ ) mixing coefficients defined in Eqs. (9) and (10) in the text.

$$\text{for } Q_1: |\psi_{\text{exc}}\rangle = \{\alpha(\rho)|10\rangle + \beta(\rho)|01\rangle\} |v'_{\text{tor}}\rangle, \quad (11)$$

$$\text{for } Q_3: |\psi_{\text{exc}}\rangle = \{-\beta(\rho)|10\rangle + \alpha(\rho)|01\rangle\} |v'_{\text{tor}}\rangle, \quad (12)$$

where  $|ij\rangle$  is the unperturbed eigenstate with vibrational quantum numbers  $\nu(Q_1)=i$ ,  $\nu(Q_3)=j$ .

From a restricted normal coordinate analysis of the OH stretching modes, one can deduce the general form of  $\alpha(\rho)$  and  $\beta(\rho)$  via the expected effect of the interaction with benzene on the force constants for the two O-H bonds. Since the force constant difference changes sign under reflection through  $\rho$ ,  $\beta(\rho)$  is odd in  $\rho$  while  $\alpha(\rho)$  is even. Furthermore,  $\beta(\rho)$  will approach zero at large angles. The general form of these functions is shown in Fig. 7. The obvious consequence of this mixing is that not only the direction, but also the magnitude of the dipole moment derivatives for the OH stretch modes changes with angle  $\rho$ .

### 4. Calculation of positions and intensities of the OH stretch infrared bands

To compare with experiment, torsion/internal rotation energy levels are calculated by diagonalizing the model Hamiltonian of ground and OH vibrationally excited states for various assumed forms of the effective  $\rho$ -dependent potential. Variables at hand are the harmonic frequency, the depth of the double minimum well, the height and width of the barrier at  $\rho=0^\circ$ , and in C<sub>6</sub>H<sub>6</sub>-HOD, its asymmetry.

Calculation of the infrared intensities of the band requires an analysis of the effects of the large-amplitude motions on the OH stretch band intensities. The intensity<sup>26</sup> of an electric dipole-allowed infrared transition of frequency  $\nu$  between  $\psi_{\text{gs}}$  and  $\psi_{\text{exc}}$  is equal to

$$I = c \left| \langle \psi_{\text{gs}} | \sum_r \left( \frac{\partial \mu}{\partial Q_r} \right) Q_r | \psi_{\text{exc}} \rangle \right|^2, \quad (13)$$

where  $c = (8\pi^3/3hc)N_{gs}\nu$  and is taken as a constant for all bands in what follows.

If the  $z$  axis is taken as the symmetric top axis (Fig. 1), then

$$I_{\parallel} = c \left| \langle \psi_{gs} | \sum_r \left( \frac{\partial \mu_z}{\partial Q_r} \right)_0 Q_r | \psi_{exc} \rangle \right|^2 \quad (14)$$

and

$$I_{\perp} = c \left| \langle \psi_{gs} | \sum_r \left( \frac{\partial \mu_x}{\partial Q_r} \right)_0 Q_r + \left( \frac{\partial \mu_y}{\partial Q_r} \right)_0 Q_r | \psi_{exc} \rangle \right|^2. \quad (15)$$

*a. C<sub>6</sub>H<sub>6</sub>-H<sub>2</sub>O.* In C<sub>6</sub>H<sub>6</sub>-H<sub>2</sub>O, the intensity of an infrared transition in the OH stretch region is given by

$$I = c \left| \langle \psi_{gd} | \left[ \left( \frac{\partial \mu}{\partial Q_1} \right) Q_1 + \left( \frac{\partial \mu}{\partial Q_3} \right) Q_3 \right] | \psi_{exc} \rangle \right|^2, \quad (16)$$

where  $Q_1$  and  $Q_3$  have been defined in Eqs. (9) and (10). It can readily be shown by use of Eqs. (9) and (10) that

$$\left( \frac{\partial \mu}{\partial Q_1} \right) Q_1 + \left( \frac{\partial \mu}{\partial Q_3} \right) Q_3 = \left( \frac{\partial \mu}{\partial Q_1^0} \right) Q_1^0 + \left( \frac{\partial \mu}{\partial Q_3^0} \right) Q_3^0, \quad (17)$$

so that Eq. (16) is more conveniently expressed as

$$I = c \left| \langle \psi_{gd} | \left[ \left( \frac{\partial \mu}{\partial Q_1^0} \right) Q_1^0 + \left( \frac{\partial \mu}{\partial Q_3^0} \right) Q_3^0 \right] | \psi_{exc} \rangle \right|^2. \quad (18)$$

The dipole moment derivatives in Eq. (18) are vector quantities. In a rigid molecule or complex, the direction of these vectors is constant. However, in the present case, where large-amplitude motion along both  $\rho$  and  $\phi$  can occur, one must explicitly take into account the dependence of the dipole moment derivative vectors on  $\rho$  and  $\phi$ . In H<sub>2</sub>O these vectors point at angle  $\rho$  (for  $Q_1^0$ ) and perpendicular to it (for  $Q_3^0$ ). Thus, the Cartesian components are given by

$$\left( \frac{\partial \mu}{\partial Q_1^0} \right) = \left( \frac{\partial \mu}{\partial Q_1^0} \right)_0 (\sin \rho \cos \phi, \sin \rho \sin \phi, \cos \rho) \quad (19)$$

and

$$\left( \frac{\partial \mu}{\partial Q_3^0} \right) = \left( \frac{\partial \mu}{\partial Q_3^0} \right)_0 (\cos \rho \cos \phi, \cos \rho \sin \phi, \sin \rho).$$

After integrating over the angle  $\phi$ , the band-integrated intensities of the parallel and perpendicular transitions are then

$$I_{\parallel} = c \left| \left( \frac{\partial \mu}{\partial Q_1^0} \right)_0 \langle \psi_{gd} | Q_1^0 \cos(\rho) | \psi_{exc} \rangle + \left( \frac{\partial \mu}{\partial Q_3^0} \right)_0 \langle \psi_{gd} | Q_3^0 \sin(\rho) | \psi_{exc} \rangle \right|^2 \quad (20)$$

and

$$I_{\perp} = 2c \left| \left( \frac{\partial \mu}{\partial Q_1^0} \right)_0 \langle \psi_{gd} | Q_1^0 \sin(\rho) | \psi_{exc} \rangle + \left( \frac{\partial \mu}{\partial Q_3^0} \right)_0 \langle \psi_{gd} | Q_3^0 \cos(\rho) | \psi_{exc} \rangle \right|^2, \quad (21)$$

where the factor of 2 in Eq. (21) relates the integrated intensity of a perpendicular transition to that of a parallel transition of same  $(d\mu/dQ)_0$  magnitude.<sup>26</sup>

For free H<sub>2</sub>O, we know that the integrated intensity of the asymmetric stretch is 20 times that of the symmetric stretch. Given the factor of 2 in Eq. (20), this means that the dipole moment derivatives are approximately related by

$$\left( \frac{\partial \mu}{\partial Q_3^0} \right)_0 = \sqrt{10} \left( \frac{\partial \mu}{\partial Q_1^0} \right)_0. \quad (22)$$

Plugging Eqs. (11), (12), and (22) into Eqs. (20) and (21), and noting that

$$\langle 00 | Q_1^0 | 10 \rangle \approx \langle 00 | Q_3^0 | 01 \rangle \equiv \xi \quad (23)$$

while

$$\langle 00 | Q_1^0 | 01 \rangle = \langle 00 | Q_3^0 | 10 \rangle = 0, \quad (24)$$

the following expressions are obtained for the parallel and perpendicular transitions in the  $Q_1$  and  $Q_3$  regions of the infrared including  $Q_1^0/Q_3^0$  mixing:

$$I_{\parallel}(Q_1) = c \left( \frac{\partial \mu}{\partial Q_1^0} \right)_0^2 \xi^2 |\langle \nu''_{\text{tor}} = 0 | [\alpha(\rho) \cos \rho + \sqrt{10} \beta(\rho) \sin \rho] | \nu'_{\text{tor}} \rangle|^2 \delta_{m'', m'}, \quad (25)$$

$$I_{\perp}(Q_1) = 2c \left( \frac{\partial \mu}{\partial Q_1^0} \right)_0^2 \xi^2 |\langle \nu''_{\text{tor}} = 0 | [\alpha(\rho) \sin \rho + \sqrt{10} \beta(\rho) \cos \rho] | \nu'_{\text{tor}} \rangle|^2 \delta_{m'', m'' \pm 1}, \quad (26)$$

$$I_{\parallel}(Q_3) = c \left( \frac{\partial \mu}{\partial Q_1^0} \right)_0^2 \xi^2 |\langle \nu''_{\text{tor}} = 0 | [-\beta(\rho) \cos \rho + \sqrt{10} \alpha(\rho) \sin \rho] | \nu'_{\text{tor}} \rangle|^2 \delta_{m'', m'}, \quad (27)$$

and

$$I_{\perp}(Q_3) = 2c \left( \frac{\partial \mu}{\partial Q_1^0} \right)_0^2 \xi^2 |\langle \nu''_{\text{tor}} = 0 | [-\beta(\rho) \sin \rho + \sqrt{10} \alpha(\rho) \cos \rho] | \nu'_{\text{tor}} \rangle|^2 \delta_{m'', m'' \pm 1}. \quad (28)$$

Here  $m''$  and  $m'$  are the internal rotation quantum numbers along  $\phi$  in ground and excited states, respectively. Expressions (25)–(28) predict the selection rules for combination bands involving torsion/internal rotation levels shown in Table I. Since  $\alpha(\rho)$  is even in  $\rho$  and  $\beta(\rho)$  is odd, parallel bands are allowed in the  $Q_1$  region with  $\Delta \nu_{\text{tor}}$  even, while perpendicular bands will have  $\Delta \nu_{\text{tor}}$  odd. In the  $Q_3$  (asymmetric stretch) region, the reverse is true; perpendicular bands are allowed with  $\Delta \nu_{\text{tor}}$  even while parallel bands require  $\Delta \nu_{\text{tor}}$  odd. As expected, the  $\sqrt{10}$  weighting of the  $\beta$  coefficient in the  $Q_1$  expressions [Eqs. (25) and (26)] means that even small mixing of  $Q_3$  with  $Q_1$  can give significant changes to the intensities of a given  $Q_1$  combination band.

It is instructive to look at the conditions under which OH stretch/torsion combination bands are weak and what conditions gives them significant intensity.

TABLE I. Selection rules for internal rotation/torsion combination bands built on the OH stretch vibrations of C<sub>6</sub>H<sub>6</sub>-H<sub>2</sub>O and C<sub>6</sub>H<sub>6</sub>-HOD.

Band type		$\Delta v_{\text{tor}}$	$\Delta m$
C <sub>6</sub> H <sub>6</sub> -H <sub>2</sub> O			
Symmetric stretch region	Parallel	even	0
	Perpendicular	odd	$\pm 1$
Asymmetric stretch region	Parallel	odd	0
	Perpendicular	even	$\pm 1$
C <sub>6</sub> H <sub>6</sub> -HOD			
OH stretch region	Parallel	no restriction	0
	Perpendicular	no restriction	$\pm 1$
OD stretch region	Parallel	no restriction	0
	Perpendicular	no restriction	$\pm 1$

(1) When  $Q_1/Q_3$  mixing is negligible [i.e., when  $\alpha(\rho)=1$ ,  $\beta(\rho)=0$ ] expressions (25)–(28) reduce to

$$I_{\parallel}(Q_1) = c \left( \frac{\partial \mu}{\partial Q_1^0} \right)^2 \xi^2 |\langle v''_{\text{tor}}=0 | \cos \rho | v'_{\text{tor}} \rangle|^2 \delta_{m'',m'}, \quad (29)$$

$$I_{\perp}(Q_1) = 2c \left( \frac{\partial \mu}{\partial Q_1^0} \right)^2 \xi^2 |\langle v''_{\text{tor}}=0 | \sin \rho | v'_{\text{tor}} \rangle|^2 \delta_{m'',m''\pm 1}, \quad (30)$$

$$I_{\parallel}(Q_3) = 10c \left( \frac{\partial \mu}{\partial Q_1^0} \right)^2 \xi^2 |\langle v''_{\text{tor}}=0 | \sin \rho | v'_{\text{tor}} \rangle|^2 \delta_{m'',m'}, \quad (31)$$

and

$$I_{\perp}(Q_3) = 20c \left( \frac{\partial \mu}{\partial Q_1^0} \right)^2 \xi^2 |\langle v''_{\text{tor}}=0 | \cos \rho | v'_{\text{tor}} \rangle|^2 \delta_{m'',m''\pm 1}. \quad (32)$$

Note that the selection rules for  $\Delta v_{\text{tor}}$  are the same in the absence of  $Q_1/Q_3$  mixing as when it is present. Consequently, the major effect of the  $Q_1/Q_3$  mixing is to change the intensities of the combination bands.

(2) Two further restrictions are required to remove combination bands from the spectra. First, if the torsional vibration is small-amplitude,  $\sin \rho$  and  $\cos \rho$  can be approximated by their values at  $\rho=\rho_0$  and pulled outside the integral. Second, if there is no coupling of the torsion to the OH stretch, the torsional wave functions will be unchanged by OH stretch excitation. Then the orthogonality of the torsional wave functions will limit transitions to those with  $\Delta v_{\text{tor}}=0$ , i.e., only OH stretch fundamentals will appear in the spectrum. This is the typical rigid molecule, harmonic oscillator result.

*b. C<sub>6</sub>H<sub>6</sub>-HOD.* The situation is very different in C<sub>6</sub>H<sub>6</sub>-HOD. Here the OH and OD stretches are local mode stretches in which the dipole moment derivatives point along the OH and OD bonds, respectively. Given the reference configuration of Fig. 1, the Cartesian components of these vectors are

$$\left( \frac{\partial \mu}{\partial Q_{\text{OH}}} \right) = \left( \frac{\partial \mu}{\partial Q_{\text{OH}}^0} \right) [\sin(\rho+52^\circ) \cos \phi, \sin(\rho+52^\circ) \sin \phi, \cos(\rho+52^\circ)] \quad (33)$$

and

$$\left( \frac{\partial \mu}{\partial Q_{\text{OD}}} \right) = \left( \frac{\partial \mu}{\partial Q_{\text{OD}}^0} \right) [\sin(\rho-52^\circ) \cos \phi, \sin(\rho-52^\circ) \sin \phi, \cos(\rho-52^\circ)]. \quad (34)$$

As before, after integrating over the angle  $\phi$ , the band-integrated intensities of the parallel and perpendicular transitions in the OH stretch region are given by

$$I_{\parallel}(Q_{\text{OH}}) = c \left( \frac{\partial \mu}{\partial Q_{\text{OH}}^0} \right)^2 \xi_{\text{OH}}^2 |\langle v''_{\text{tor}}=0 | \cos(\rho+52^\circ) | v'_{\text{tor}} \rangle|^2 \delta_{m'',m'} \quad (35)$$

and

$$I_{\perp}(Q_{\text{OH}}) = 2c \left( \frac{\partial \mu}{\partial Q_{\text{OH}}^0} \right)^2 \xi_{\text{OH}}^2 |\langle v''_{\text{tor}}=0 | \sin(\rho+52^\circ) | v'_{\text{tor}} \rangle|^2 \times \delta_{m'',m''\pm 1}. \quad (36)$$

The analogous expressions for the OD stretch transitions substitute  $(\rho-52^\circ)$  for  $(\rho+52^\circ)$ .

Note that in C<sub>6</sub>H<sub>6</sub>-HOD there is no definite parity to the  $\rho$ -dependent integrand and  $\Delta v_{\text{tor}}$  is not restricted to even or odd as it is in the H<sub>2</sub>O case. In particular, both  $\Delta v_{\text{tor}}=0$  and 1 are allowed and may be strong. Furthermore, we anticipate that both parallel and perpendicular transitions out of the ( $v''_{\text{tor}}=0$ ,  $m''=0$ ) level will carry significant intensity.

## C. The comparison with experiment

### 1. C<sub>6</sub>H<sub>6</sub>-HOD

Our goal in modeling the C<sub>6</sub>H<sub>6</sub>-HOD spectrum is to account for the highly unusual intensity profile of the OH stretch transitions in which combination bands are significantly more intense than the OH stretch fundamental. Figure 8(b) presents a calculated fit to the experimental spectrum of C<sub>6</sub>H<sub>6</sub>-HOD [Fig. 8(a)] which is representative of the quality of fit possible with this model. As can be seen from the figure, the 2D LAM model is capable of correctly reproducing the experimental intensity profile. The  $\rho$ -dependent potentials associated with the calculated spectrum are shown in Fig. 9. Given the number of parameters in the model (the height, width, and asymmetry in both ground and excited states), the precise form of the potential cannot be deduced uniquely from the present data. However, certain features of the potentials are present in all satisfactory fits.

(1) To correctly reproduce the relative intensities in the spectrum, it is necessary to assign the transitions as shown in the figure; namely, with the  $\Sigma(0)$ - $\Sigma(1)$  transition below the  $\Sigma(0)$ - $\Pi(0)$  transition. Here the transition labels are  $m''(v''_{\text{tor}}) \rightarrow m'(v'_{\text{tor}})$ .

(2) In order to obtain a 10 cm<sup>-1</sup> torsion fundamental, a harmonic torsional frequency of about 20 cm<sup>-1</sup> is required, and a small barrier of about 20–30 cm<sup>-1</sup> needs to be placed in the potential at  $\rho=0^\circ$ . This results in a broad, flat torsional

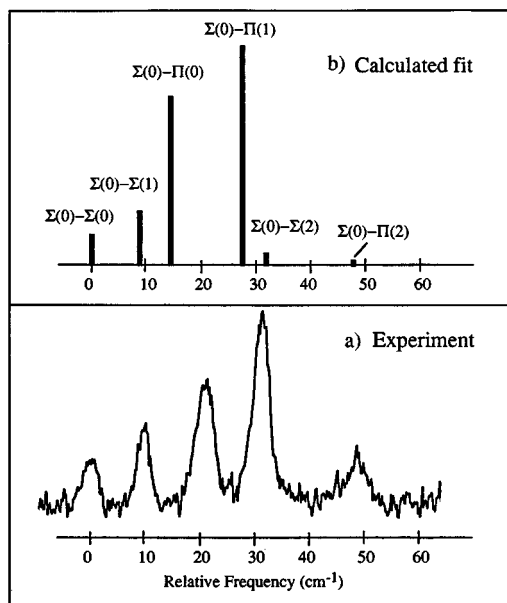


FIG. 8. (a) The experimental C<sub>6</sub>H<sub>6</sub>-HOD RIDIR spectrum in the OH stretch region and (b) a calculated fit using the 2D ( $\rho, \phi$ ) model described in the text which is representative of the quality of fit possible with this model. The assignments for the transitions are of the form [ $m''(v''_{\text{tor}}) - m'(v'_{\text{tor}})$ ], where  $m$  is the internal rotor quantum number in  $\phi$  ( $m=0 \leftrightarrow \Sigma$  and  $m=1 \leftrightarrow \Pi$ ) and  $v_{\text{tor}}$  is the vibrational quantum number in torsion along  $\rho$ .

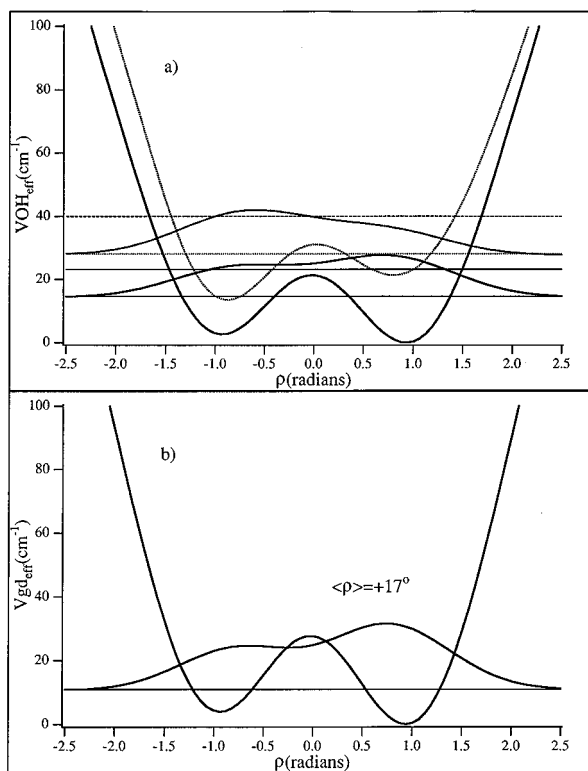


FIG. 9. Plots of  $V_{\text{eff}}(\rho)$  for the  $v_{\text{OH}}=0$   $\Sigma$  ground state, the  $v_{\text{OH}}=1$   $\Sigma$  state, and the  $v_{\text{OH}}=1$ ,  $\Pi$  state of C<sub>6</sub>H<sub>6</sub>-HOD which produce the calculated OH stretch infrared spectrum in Fig. 8(b). The first few energy levels and  $v_{\text{tor}}=0$  wave functions are also shown.

potential in which the binding energy of the HOD molecule with the benzene ring changed by less than 50 cm<sup>-1</sup> over changes in  $\rho$  from -90 to +90 deg.

(3) The spacing between  $\Sigma(0)-\Sigma(0)$  and  $\Sigma(0)-\Pi(0)$  transitions is fixed by the  $\rho$ -dependent potential and the assumption of free internal rotation about  $\phi$ , and is not a free parameter. Its typical value is 14 cm<sup>-1</sup>, compared to 20 cm<sup>-1</sup> in the experimental spectrum. This is perhaps the weakest aspect of the fit with this model, and likely points to the need for future refinement of the model.

(4) The qualitative experimental intensity profile can be reproduced even without any asymmetry in  $V_{\text{eff}}(\rho)$ . However, the best match-ups with experiment occurred when a small asymmetry was added to the ground state potential favoring D down. The ground state potential in Fig. 8(a) gives  $\langle \rho \rangle = +17$  deg, a value in agreement with that determined for the ground state of C<sub>6</sub>H<sub>6</sub>-HOD (18 deg) by Gutowsky *et al.*<sup>4</sup> from their microwave data. This value for  $\langle \rho \rangle$  was used as a further parameter in constraining the “best fit”  $V_{\text{eff}}(\rho)$ .

## 2. C<sub>6</sub>H<sub>6</sub>-H<sub>2</sub>O

Given the broad, flat potential in  $\rho$  derived from the fit to experiment for C<sub>6</sub>H<sub>6</sub>-HOD, it is important to check the effects of a similarly broad torsional potential on the C<sub>6</sub>H<sub>6</sub>-H<sub>2</sub>O spectrum. One must keep in mind that, due to  $\rho$ -dependent zero-point effects of the OH stretch vibrations and of the other intermolecular modes (Sec. IV C 2),  $V_{\text{pert}}(\rho)$  may be different for H<sub>2</sub>O than for HOD and for symmetric stretch H<sub>2</sub>O than for asymmetric stretch H<sub>2</sub>O.

As we have already seen, the dominant features of the spectra of C<sub>6</sub>H<sub>6</sub>-H<sub>2</sub>O are well-fit simply by assuming 1D free internal rotation along  $\phi$ . In fact, the OH stretch infrared spectra of C<sub>6</sub>H<sub>6</sub>-H<sub>2</sub>O hold little promise for providing detailed information about the torsional potential, since the  $Q_3$  region shows only weak combination bands, while no additional structure is detectable in the  $Q_1$  region. The goal of applying the 2D model to C<sub>6</sub>H<sub>6</sub>-H<sub>2</sub>O is then to account in a consistent way for the *presence* of the small additional transitions in the asymmetric stretch region and the *absence* of such transitions in the symmetric stretch region.

Figure 10 displays a stick diagram of the experimental and a calculated spectrum in the asymmetric stretch region. The several small transitions not explained by the 1D free internal rotation model are qualitatively accounted for within the 2D ( $\rho, \phi$ ) model as combination bands involving the torsion. If a harmonic frequency consistent with the C<sub>6</sub>H<sub>6</sub>-HOD potential is retained, an excited state barrier of 20 cm<sup>-1</sup> at  $\rho=0^\circ$  is required to bring the combination bands into the region where they are observed experimentally. The form of the potentials associated with the calculated spectrum is shown in Figs. 11(a) and 11(b). A small amount of  $Q_1/Q_3$  mixing is included in the calculated spectrum, to be consistent with the results on the  $Q_1$  region which follow. However, little change in the asymmetric stretch spectrum is induced by changes in the amount of  $Q_1/Q_3$  mixing or even its complete neglect.

The symmetric stretch region is more interesting. Here no combination bands are observed in the spectrum [Figs. 3

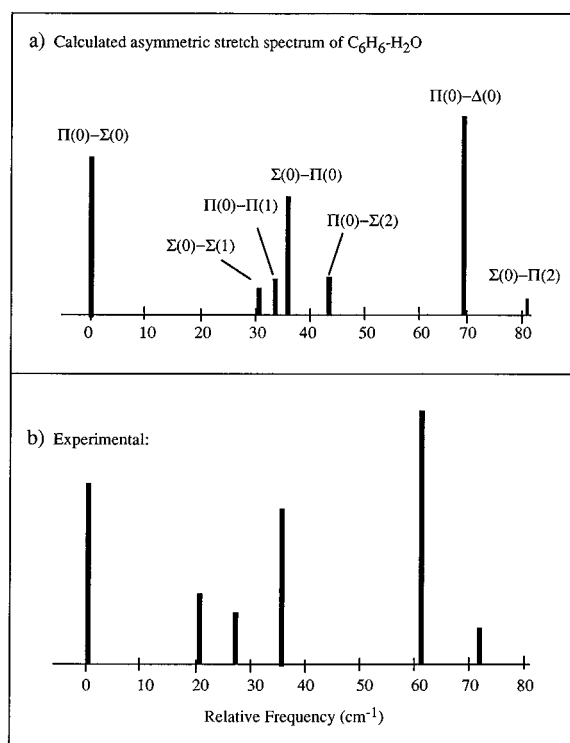


FIG. 10. Stick diagrams of the (a) experimental and (b) calculated spectra in the asymmetric stretch region of C<sub>6</sub>H<sub>6</sub>-H<sub>2</sub>O using the potentials in Figs. 11(a) and 11(b).

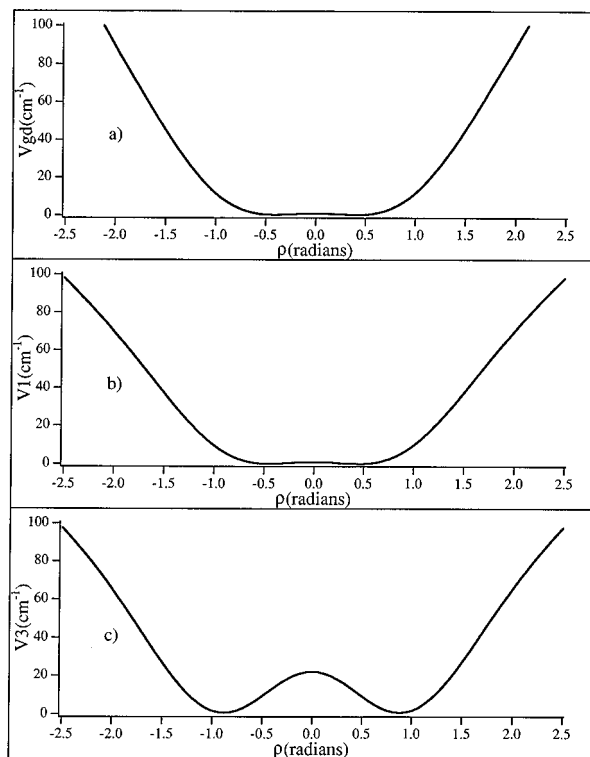


FIG. 11.  $V_{\text{eff}}(\rho)$  in the (a) ground, (b) symmetric stretch, and (c) asymmetric stretch vibrationally excited states in the calculated spectra of Figs. 10(b) and 12(b)–12(f).

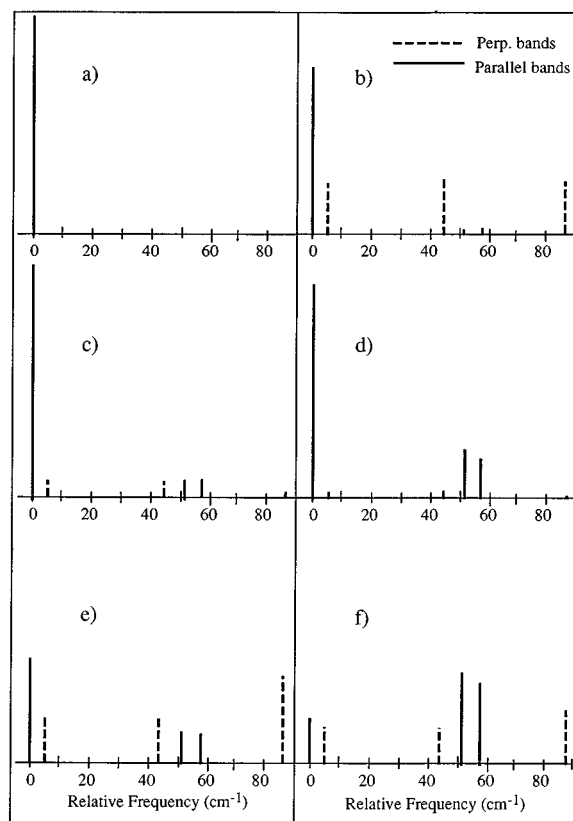


FIG. 12. Stick diagrams of the (a) experimental and (b)–(f) calculated spectra in the symmetric stretch region of C<sub>6</sub>H<sub>6</sub>-H<sub>2</sub>O using the potentials in Figs. 11(a) and 11(c). The calculated spectra of (b)–(f) use  $Q_1$ - $Q_3$  mixing coefficients  $\alpha(\rho)$  and  $\beta(\rho)$  of the general form shown in Fig. 7, where (b)  $\beta=0$ , i.e., no  $Q_1/Q_3$  mixing, (c)  $\beta(\rho_{\text{max}})=0.25$ ,  $\rho_{\text{max}}=30^\circ$ , (d)  $\beta(\rho_{\text{max}})=0.25$ ,  $\rho_{\text{max}}=30^\circ$ , (e)  $\beta(\rho_{\text{max}})=0.50$ ,  $\rho_{\text{max}}=52^\circ$ , and (f)  $\beta(\rho_{\text{max}})=0.50$ ,  $\rho_{\text{max}}=52^\circ$ . The most effective suppression of combination bands occurs for the conditions of (c).

and 12(a)]. Admittedly, the lower inherent strength of the symmetric stretch transition may hinder the observation of the combination bands in the present experiment. However, the saturation present in the experimental spectrum suggests that they should be observable if present. More importantly, calculations employing a flat, broad torsional potential without  $Q_1/Q_3$  mixing predict strong symmetric stretch/torsion combination bands such as those shown in Fig. 12(b). This is true for all reasonable forms of  $V_{\text{eff}}(\rho)$ . Thus, to account for the qualitative appearance of the spectrum in this region consistently with the C<sub>6</sub>H<sub>6</sub>-HOD results, one must invoke some degree of  $Q_1/Q_3$  mixing (Sec. IV C 3).

Figures 12(c)–12(f) show the computed symmetric stretch spectrum for several representative forms of  $\beta(\rho)$ . The effect of this mixing on the appearance of the spectrum is dramatic. As the magnitude and width of  $\beta(\rho)$  changes, intensity is given preferentially either to parallel  $\Delta v_{\text{tor}}=2$  transitions or perpendicular  $\Delta v_{\text{tor}}=1$  transitions. Of the  $\beta(\rho)$  functional forms searched, that used in calculating the spectrum in Fig. 12(c) most effectively suppresses both these types of combination bands relative to the main  $\Sigma$ - $\Sigma$  and  $\Pi$ - $\Pi$  transitions. The explicit form of  $\beta(\rho)$  for this case is shown in Fig. 7. In the calculated spectra of Figs. 12(b)–

12(f), the single set of potentials shown in Figs. 11(a) and 11(c) are used. Based on the present data, the precise form of the  $V_{\text{eff}}(\rho)$  can be chosen with some degree of latitude. The potentials of Fig. 11 are simply a consistent set whose shape contributes to the strong suppression of combination bands in the symmetric stretch region shown in Fig. 12(c). A calculation using the  $Q_3$  potential of Fig. 11(b) on the  $Q_1$  region gives combination bands about twice the size shown in Fig. 12(c).

The maximum value of  $\beta$  used in calculating Fig. 12(c) is  $\beta_{\text{max}}=0.25$ , corresponding to 5%  $Q_3^0/95\%$   $Q_1^0$  mixture in  $Q_1$  at  $\rho_{\text{max}}$ . As stated previously, a mixing this small has such a dramatic effect on  $Q_1$  due to the much stronger absorption strength of  $Q_3^0$  relative to  $Q_1^0$ . From a physical standpoint, this mixing rotates the orientation of  $(\delta\mu/\delta Q_1)$  away from H<sub>2</sub>O's  $C_{2v}$  axis. As H<sub>2</sub>O rocks away from the symmetric  $\rho=0$  position to either side, mixing with  $Q_3^0$  causes the dipole derivative vector to remain oriented close to benzene's sixfold axis over a significant range of  $\rho$ , thus minimizing the perpendicular transitions in the spectrum. Put another way, the partial local mode character induced by the mixing swings the dipole derivative vector toward the OH bond pointing toward the ring.

## V. DISCUSSION AND CONCLUSIONS

The intent of the present study has been to use the OH stretch infrared spectrum as a probe of the  $\pi$  hydrogen bond between H<sub>2</sub>O (HOD) and C<sub>6</sub>H<sub>6</sub>. These spectra show sensitivity to perhaps the most striking feature of this  $\pi$  hydrogen bond; namely, the facile, large-amplitude tumbling of H<sub>2</sub>O and HOD on benzene's surface.

The observable consequences of the LAMs on the spectra change dramatically from H<sub>2</sub>O symmetric stretch to asymmetric stretch and from H<sub>2</sub>O to HOD. In fact, the three spectral regions span an interesting range of possibilities:

- (1) In the C<sub>6</sub>H<sub>6</sub>-H<sub>2</sub>O symmetric stretch region, no combination bands are observed in the spectrum.
- (2) In the C<sub>6</sub>H<sub>6</sub>-H<sub>2</sub>O asymmetric stretch region, at least six bands are observed. The three dominant bands are readily assigned as perpendicular bands of an internally rotating symmetric top while the three weak transitions appear to be OH stretch/torsion/internal rotation combination bands.
- (3) In the C<sub>6</sub>H<sub>6</sub>-HOD OH stretch region, five transitions are observed out of the zero point level of the ground state, with OH stretch/torsion/internal rotation combination bands dominating the spectrum, with intensities several times that of the fundamental.

The sensitivity of the spectra to isotopic substitution (H<sub>2</sub>O to HOD) is a direct consequence of the fundamental change in the form of the O-H(D) stretching modes accompanying the substitution. As summarized in Fig. 13, the isotopic substitution changes

- (1) the form of the normal coordinates from modes delocalized over both bonds in H<sub>2</sub>O to localized in a single bond in HOD;

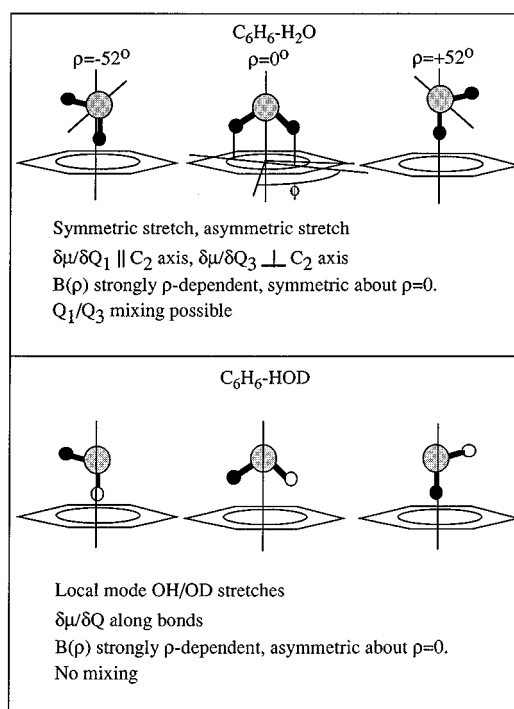


FIG. 13. Summary of the fundamental differences between H<sub>2</sub>O and HOD which influence the appearance of the OH stretch infrared spectra of C<sub>6</sub>H<sub>6</sub>-H<sub>2</sub>O and C<sub>6</sub>H<sub>6</sub>-HOD complexes undergoing 2D LAM in  $\rho$  and  $\phi$ .

- (2) the direction of the dipole moment derivatives from parallel and perpendicular to the  $C_{2v}$  axis of H<sub>2</sub>O to along the OH and OD bonds in HOD;
- (3) the form of the  $\rho$ -dependent internal rotation constant  $F(\rho)$  from symmetric about  $\rho=0^\circ$  in H<sub>2</sub>O to distinctly asymmetric in HOD;
- (4) the degree of  $\rho$ -dependent mixing between the hydride stretch modes from significant in H<sub>2</sub>O to insignificant in HOD.

When combined with the large-amplitude motions in  $\rho$  and  $\phi$ , these changes lead to the observed differences in the spectra. The modeling of the infrared spectra including large-amplitude motions in  $\rho$  and  $\phi$  successfully accounts for the qualitative features of the spectrum of C<sub>6</sub>H<sub>6</sub>-HOD, including the unusual intensity profile and approximate positions of the observed bands.

The  $\rho$ -dependent potential so derived is indeed remarkably broad, with the HOD molecule undergoing orientational changes from  $\rho=-90^\circ$  to  $+90^\circ$  even at the zero point level (Fig. 9).

While the present level of analysis seems appropriate to the data available in this study, it also points out the need for further study before a quantitatively accurate C<sub>6</sub>H<sub>6</sub>-H<sub>2</sub>O intermolecular potential is in hand. On the experimental side, similar spectra in the OD stretch region of C<sub>6</sub>H<sub>6</sub>-HOD would provide an excellent testing ground for further refinement of  $V_{\text{eff}}(\rho)$ . Second, rotationally resolved spectra, if lifetime broadening is not too great, would provide crucial further tests. Third, far infrared spectra which sample other intermolecular degrees of freedom are needed. Fourth, an

accurate measurement of the C<sub>6</sub>H<sub>6</sub>-H<sub>2</sub>O binding energy is still not available.

From a theoretical viewpoint, modeling which includes other intermolecular degrees of freedom is needed; most notably, the third internal rotation coordinate  $\chi$  and the bending modes. It is the authors' opinion that the in-plane torsion along  $\rho$  may be strongly coupled to the in-plane bending mode, as suggested by recent MMC (Ref. 8) and *ab initio*<sup>3,10</sup> calculations. Such coupling is not included in the present analysis. Finally, a more thorough analysis of the  $\rho$ -dependent  $Q_1/Q_3$  mixing may shed additional light on the unique dynamical processes involved the tumbling of water on an aromatic surface. The present results and their relevance to water molecule's physisorption on graphite (and even metal) surfaces also deserve further exploration.

*Note added in proof.* Recent *ab initio* calculations on C<sub>6</sub>H<sub>6</sub>-H<sub>2</sub>O at the MP2 level predict that, in the presence of benzene, the intensities of the asymmetric and symmetric stretches are in the ratio  $I_{\text{asym}}/I_{\text{sym}}=1.5$  rather than 20, as it is in free H<sub>2</sub>O. This intensity change, not incorporated in the present analysis, is consistent with the intensity ratio observed in the experimental spectrum of Fig. 3(a). The physical reason for the remarkable sensitivity of the symmetric and asymmetric stretch intensities to external perturbation is currently being explored.

## ACKNOWLEDGMENTS

The authors gratefully acknowledge the National Science Foundation (NSF-CHE9404716) for their support of this research. An equipment grant from Continuum, Inc. to build the OPO is also gratefully acknowledged. T. S. Z. thanks the University of Colorado for a Joint Institute for Laboratory Astrophysics Visiting Fellowship for 1994-95 and David Nesbitt and Joel Bowman for many essential discussions on the effects of large-amplitude motions on infrared spectra.

<sup>1</sup>A. Engdahl and B. Nelander, *J. Phys. Chem.* **89**, 2860 (1985).

<sup>2</sup>A. J. Gotch and T. S. Zwier, *J. Chem. Phys.* **96**, 3388 (1992); A. W. Garrett and T. S. Zwier, *ibid.* **96**, 3402 (1992); a review chapter to appear in *Advances in Multiphoton Processes and Spectroscopy*, edited by S. H. Lin, A. A. Villaeys, and Y. Fujimara (to be published).

<sup>3</sup>S. Suzuki, P. G. Green, R. E. Bumgarner, S. Dasgupta, W. A. Goddard III, and G. A. Blake, *Science* **257**, 942 (1992).

<sup>4</sup>H. S. Gutowsky, T. Emilsson, and E. Arunan, *J. Chem. Phys.* **99**, 4883 (1993).

<sup>5</sup>J. Wanna, J. A. Menapace, and E. R. Bernstein, *J. Chem. Phys.* **85**, 1795 (1986).

<sup>6</sup>P. M. Felker (private communication).

<sup>7</sup>P. Linse, *J. Comput. Chem.* **9**, 505 (1988).

<sup>8</sup>J. D. Augspurger, C. E. Dykstra, and T. S. Zwier, *J. Phys. Chem.* **96**, 7257 (1992).

<sup>9</sup>J. D. Augspurger, C. E. Dykstra, and T. S. Zwier, *J. Phys. Chem.* **97**, 980 (1993).

<sup>10</sup>G. Karlstrom, P. Linse, A. Wallqvist, and B. Jonsson, *J. Am. Chem. Soc.* **105**, 3777 (1983); P. Linse, G. Karlstrom, and B. Jonsson, *ibid.* **106**, 4096 (1984); P. Linse, *J. Chem. Phys.* **86**, 4177 (1987).

<sup>11</sup>G. C. Pimentel and A. L. McClellan, *The Hydrogen Bond* (Freeman, San Francisco, 1960).

<sup>12</sup>See, for example, J. G. C. M. van Duijneveldt-van de Rijdt and F. B. van Duijneveldt, *J. Comput. Chem.* **13**, 399 (1992).

<sup>13</sup>S. Fredericks, K. Jordan, and T. Zwier (unpublished results).

<sup>14</sup>R. N. Pribble and T. S. Zwier, *Science* **265**, 75 (1994).

<sup>15</sup>R. N. Pribble and T. S. Zwier, *Faraday Discuss.* (to be published).

<sup>16</sup>E. Honegger and S. Leutwyler, *J. Chem. Phys.* **88**, 2582 (1988).

<sup>17</sup>The assignment of the water dimer donor OH stretch transition has recently been revised by F. Huisken, M. Kaloudis, and A. Kulcke, *Faraday Discuss.* **97**, 319 (1994). The other three bands were assigned previously by Z. S. Huang and R. E. Miller, *J. Chem. Phys.* **91**, 6613 (1989). The assignments are donor stretch free O-H (3730 cm<sup>-1</sup>), donor bonded O-H (3554 cm<sup>-1</sup>), acceptor asymmetric stretch (3745.48 cm<sup>-1</sup>), and acceptor symmetric stretch (3600 cm<sup>-1</sup>).

<sup>18</sup>R. C. Cohen, K. L. Busarow, K. B. Laughlin, G. A. Blake, M. Havenith, Y. T. Lee, and R. J. Saykally, *J. Chem. Phys.* **89**, 4494 (1988); R. C. Cohen, K. L. Busarow, Y. T. Lee, and R. J. Saykally, *ibid.* **92**, 169 (1990).

<sup>19</sup>S. Suzuki, R. E. Bumgarner, P. A. Stockman, P. G. Green, and G. A. Blake, *J. Chem. Phys.* **94**, 824 (1991).

<sup>20</sup>R. Lascola and D. J. Nesbitt, *J. Chem. Phys.* **95**, 7917 (1991).

<sup>21</sup>J. D. Augspurger and C. E. Dykstra (unpublished results).

<sup>22</sup>G. Herzberg, *Molecular Spectra and Molecular Structure* (Van Nostrand, Princeton, 1945), Vol. II, pp. 491ff.

<sup>23</sup>G. V. Hartland, B. F. Henson, V. A. Ventura, and P. M. Felker, *J. Phys. Chem.* **96**, 1164 (1992).

<sup>24</sup>K. N. Rao, in *Molecular Spectroscopy: Modern Research*, edited by K. N. Rao (Academic, New York, 1976), Vol. II, pp. 165ff. The 20-fold difference in intensity between asymmetric and symmetric stretch modes is a consequence of the nonlinear dependence of  $\mu$  on  $Q$ . If  $d\mu/dR_{\text{OH}}$  were constant over the  $R_{\text{OH}}$ 's sampled during vibration, simple geometry would predict  $I_{\text{asym}}/I_{\text{sym}}=3.5$ .

<sup>25</sup>F. Culot and J. Lievin, *Phys. Scr.* **46**, 502 (1992).

<sup>26</sup>E. B. Wilson, Jr., J. C. Decius, and P. C. Cross, *Molecular Vibrations* (Dover, New York, 1955), pp. 162ff.